

Cold-Set Whey Protein Gels with Addition of Polysaccharides

Ângelo Luiz Fazani Cavallieri · Rosiane Lopes Cunha

Received: 4 August 2008 / Accepted: 26 February 2009 / Published online: 14 March 2009
© Springer Science + Business Media, LLC 2009

Abstract Cold-set whey protein (WP) gels with addition of xanthan or guar were evaluated by mechanical properties and scanning electron microscopy. Gels were formed after the addition of different amounts of glucono- δ -lactone to thermally denatured WP solutions, leading to different acidification rates and final pH values. At lower acidification rates and higher final pH, gels showed more discontinuous structure and weaker and less elastic network, which was attributed to a predominance of phase separation during gel formation due to slower gelation kinetics. In contrast, at higher acidification rates and lower final pHs, gelation prevailed over phase separation, favoring the formation of less porous structures, resulting in stronger and more elastic gels. The gels' fractal dimension (D_f ; structure complexity) and lacunarity were also influenced by the simultaneous effects of gelation and phase separation. For systems where phase separation was the prevailing mechanism, greater lacunarity parameters were usually observed, describing the heterogeneity of pore distribution, while the opposite occurred at prevailing gelation conditions. Increase in guar concentration or lower final pH of xanthan gels entailed in D_f reduction, while the increase in xanthan concentration resulted in higher D_f . Such a result suggests that the network contour length was rugged, but this pattern was reduced by the increase of electrostatic interactions among WP and xanthan. Guar addition caused the formation of gel network with smoother surfaces, which could be attributed to the guar-protein excluded volume effects leading to an increase in protein-protein interactions.

Keywords Whey proteins · Glucono- δ -lactone · Cold gelation · Image analysis · Fractal · SEM · Microstructure · Xanthan · Guar

Introduction

Heating a globular protein solution causes aggregation of protein molecules by mechanisms such as hydrophobic interaction, disulfide bond formation, or electrostatic interaction, and a gel can be formed if the protein concentration is sufficiently high.¹ However, the combined control of globular protein heat denaturation and the solvent quality can also lead to a gelling process called “cold gelation”.² The advantages of cold gelation processes are the induction of gelation of globular protein at lower protein concentration and lower temperatures, allowing the addition of thermolabile compounds in the gel matrix. The cold gelation process consists of two consecutive steps. In the first step, the solution of proteins is heated at neutral pH, low ionic strength, and a protein concentration lower than the minimum required for thermal gelation, leading to a loss of their native structure with partial unfolding and subsequent aggregation. Despite this aggregation, the proteins remain soluble after cooling and do not gel due to predominant electrostatic repulsive forces amongst the aggregates formed. In the second step, changes in solvent quality reduced electrostatic repulsion among the protein aggregates and induced gelation by promoting hydrophobic interactions. Such modifications can be achieved by salt addition or system acidification towards the protein's pI . The structure and properties of cold-set protein gels depend on the gelation kinetics, type of induction (salt or acidic), and the properties of the protein aggregates formed in the first heating step as a consequence of the temperature and heating time.³

Â. L. F. Cavallieri · R. L. Cunha (✉)
Department of Food Engineering, Faculty of Food Engineering,
University of Campinas (UNICAMP),
P.O. Box 6121, 13083-862 Campinas, SP, Brazil
e-mail: rosiane@fea.unicamp.br

Even though a lot of effort has been put into understanding the cold gelation of pure protein systems,^{4–6} very few studies deal with cold gelation of mixed protein–polysaccharide systems. However, the addition of polysaccharides can also interfere in the microscopic structure of the protein gels due to specific interactions between these two biopolymers. In solution, the proteins can show attraction or repulsion with the polysaccharides depending on their origin, concentration, system pH, ionic strength, and temperature.⁷ In these systems, three possible situations may occur: (1) incompatibility, when a segregation of the biopolymers occurs in two different aqueous immiscible phases; (2) complex coacervation that arises due to a strong attraction between two different charged biopolymers forming an immiscible biopolymer complex that exudates the solvent to another phase; and (3) miscibility, when the biopolymers are homogeneously dispersed through the system.⁷

The cold-set gelation of whey protein isolate with addition of polysaccharides differing in their net charges, including xanthan and galactomannans, was recently performed.^{8,9} The gelation was induced at a fixed acid precursor concentration that led to protein gels with final pH value around 4.8 after 20 h of gel incubation at 25 °C.^{8,9} The mechanical properties of the gels were dependent on the charge density of the polysaccharide used, leading to the formation of protein-rich zones in gel microstructure with depleted polysaccharide zones.⁹ The mechanism behind the microstructure of such systems was a consequence of simultaneous phase separation and aggregation induced by acidification.⁸ Concerning pure whey protein systems at similar acidification conditions, we previously observed that the gels produced at slower acidification rates are stronger than gels formed at faster acidification conditions.¹⁰ Such behavior was related to the formation of S–S bonds amongst protein aggregates even before the achievement of the gel state.^{4,11,12} For this reason, it is important to evaluate the effects of acidification condition on microstructure properties of mixed whey protein–polysaccharide systems.

Xanthan and guar are widely used polysaccharides in the food industry as a stabilizer and thickener of food products, and they have the common characteristic of non-gelling polysaccharides.^{13,14} Xanthan is a high-molecular-weight anionic polysaccharide, and this polymer consists of a linear (1-4)- β -D glucose backbone with a charged trisaccharide side chain on each second glucose residue. The galactomannans are neutral polysaccharides, and its molecular structure generally consists in chains of mannose residues with randomly attached galactose units as side chains. Guar gum is the most widely used galactomannan due to its ability, at relatively low concentrations, to form very viscous solutions that are only slightly affected by pH, added ions, and heat processing.

In this study, our objective was to evaluate the microstructure of cold-set whey protein gels at different final pH

values with addition of two different charge density polysaccharides (guar and xanthan). The microstructure was evaluated by scanning electron microscopy (SEM) micrographs, which were related to the gels' mechanical properties. We also attempted to describe the great variety of structures obtained in SEM with an image analysis procedure, which permitted the characterization of the structure of the different gels by an objective parameter that was related to the biopolymers interactions in each system.

Materials and Methods

Materials

The whey protein isolate (WPI) Lactoprodan was obtained from ARLA FOODS INGREDIENTS (Denmark). Xanthan and glucono- δ -lactone (GDL) were obtained from Sigma Aldrich Corporation (St. Louis, USA) and guar HIGUM 55 was obtained from Rhodia Food (Brazil). According to sodium dodecyl sulfate–polyacrylamide gel electrophoresis (SDS-PAGE) experiments,¹⁵ the WPI comprised mainly β -Lg (52%), α -La (18%), and bovine serum albumin (BSA, 6%) as determined by densitometry. The lactose content in WPI powder was 0.6%, as determined by phenol sulfuric method.¹⁶ The WPI, xanthan, and guar powders were characterized by atomic absorption spectroscopy, and the following composition of ions was obtained: Na⁺ 0.63%, Ca²⁺ 0.05%, and K⁺ 0.65% for WPI, Na⁺ 2.60%, Ca²⁺ 0.40%, and K⁺ 4% for xanthan, and Na⁺ 0.051%, Ca²⁺ 0.038%, and K⁺ 0.131% for guar. The protein¹⁷ ($N \times 6.38$) and moisture content (w/w wet basis) were 92.4% and 5.7% for WPI powder, 0.65% and 8.7% for xanthan, and 4.38% and 2.3% for guar.

Preparation of Biopolymer Stock Solutions

WPI stock solutions were prepared (10%, w/w) by dissolution of the powder in deionized distilled water (pH 6.7) under a magnetic stirring for 90 min at room temperature. This solution was kept overnight at 10 °C to promote complete protein solubilization. The WPI stock solutions were then subjected to a heat treatment at 80 °C for 30 min in a stainless steel jacket vessel with mild mechanical agitation. Thermal denatured whey protein stock solution was then rapidly cooled to 10 °C in an ice bath prior to mixing with the polysaccharide stock solution. SDS-PAGE experiments were performed and results indicated the formation of protein aggregates with molecular mass superior than 200 kDa.¹²

Xanthan and guar stock solutions (1.5%, w/w) were prepared by dissolution of the powder in deionized distilled water using a strong mechanical agitation for 90 min at

room temperature (25 °C). After this step, guar stock solution was also heated at 80 °C for 30 min to promote complete polysaccharide solubilization. The pHs of polysaccharides stock solutions were measured and provided the following results: 4.73 for xanthan and 6.7 for guar. Such solutions were used in the mixed systems preparation without pH adjustment. These polysaccharide stock solutions were then rapidly cooled to 10 °C in an ice bath and kept overnight at this temperature prior to mix with the protein solution.

Preparation of the Gels: GDL-Induced Acidification

The mixed solutions were prepared in a fixed 5% (w/w) WPI content and varied polysaccharide content (% w/w): 0 (no polysaccharide addition), 0.1, 0.3, and 0.5. The stock solution aliquots were mixed and homogenized by a magnetic stirrer for at least 2 h before the addition of the water. GDL powder was pre-dissolved in this dilution water at 10 °C just before being added to the mixtures, which were gently stirred for an additional 1 min. The GDL used in each formulation was related to the protein concentration in the mixtures (GDL/WPI—w/w% ratio, R_{GDL}), which were determined in preliminary experiments in order to obtain the desired pH values after 48 h of storage at 10 °C (Table 1).

Just after the addition of GDL to the protein/polysaccharide mixtures, a part of the solutions was gently poured into small plastic tubes of dimensions of 20-mm internal diameter and 25-mm height that were sealed in order to avoid evaporation during storage. Another part was poured in thin layers into sealed small Petri dishes. Both solutions were at ambient temperature, and just after the GDL addition, they were rapidly cooled at 10 °C (around 2 min using a ice bath) and were stored at the same temperature during 48 h. The gels obtained were removed from the plastic tubes and used in compression experiments (“Mechanical Properties”) or were gently removed from the Petri dishes and then cut into small pieces (10×3×1 mm) using a sharp blade. These small pieces were then fixed in the buffers for SEM experiments (“Scanning Electron Microscopy”). Composite xanthan gels (0.1%) at pH 5.2 were removed from the plastic tubes and cut in order to separate the two gel phases. After that, these small pieces followed the same procedure described before for the microscopy experiments.

Mechanical Properties

Mechanical properties were studied using a TA-XTIII Texture Analyzer (Stable Microsystems Ltd., Surrey, England) with a 25-kg load cell. The cylindrical gels were compressed in order to determine mechanical properties under uniaxial compression. Gels were compressed with an acrylic cylindrical plate of 45-mm diameter previously lubricated with silicon oil to avoid friction between surfaces in contact. Rupture point was determined at 10 ± 1 °C by compressing the gels to 80% of their initial height using a crosshead speed of 1 mm/s. The force and height values obtained were transformed into true stress (σ_{H})—true strain (ϵ_{H}) curves.¹⁸ The rupture properties were associated with the first rupture point (usually maximum peak) of the stress–strain curve, and the Young modulus (E) was the slope of the first linear interval in the stress–strain curve and the maximum limit considered was 5% of deformation from initial sample height.

Scanning Electron Microscopy

Samples (10×3×1 mm) of gels were fixed in 2.5% glutaraldehyde in 0.1 M cacodylate buffer (pH 7.2) overnight. After being rinsed twice in cacodylate buffer, the samples were fractured under liquid nitrogen and post-fixed in 1% buffered osmium tetroxide for 2.5 h. The fixed samples were rinsed again three times with cacodylate buffer. The fractured gels were then dehydrated in a graded ethanol series (30%, 50%, 70%, and 90%). Dehydration was continued in 100% ethanol (three changes over 1 h) followed by critical point drying (Critical Point Dryer CPD03 Balzers, Alzenau, Germany). The dried samples were mounted on aluminum stubs and coated with gold in a Sputter Coater SCD 050-Balzers (Alzenau). At least seven images of typical structures at a magnification of ×500 were obtained. Images were captured using a JEOL JSM 5800 LV (Tokyo, Japan) operated at 10 kV.

Evaluation of Fractal Dimension (D_f) and Lacunarity (Λ) from the SEM Images

The microscopy images were analyzed with the public domain software ImageJ v1.38x (<http://rsb.info.nih.gov/ij/>)

Table 1 GDL/WPI ratio (R_{GDL}) for each correspondent pH after 48 h of storage at 10 °C

pH after 48h at 10 °C	R_{GDL}		
	WPI pure gels	WPI/xanthan mixed gels	WPI/guar mixed gels
5.2	0.084	0.084	0.084
4.7	0.135	0.135	0.135
4.2	0.220	0.350	0.228

and the FracLac v2.5-1d plug-in for ImageJ (<http://rsb.info.nih.gov/ij/plugins/fraclac.html>). Micrographs were transformed into 8-bit grayscale images of 640–480 pixels and were then thresholded. The gray level used for thresholding was the median of the gray level histogram of each image.¹⁹ After that, D_f values of the structure aggregates were calculated using the box counting method.²⁰ The basis of the box counting method is the placement of several grids of decreasing size over an image, and the number of boxes containing pixels (foreground pixels) is counted for each grid. The D_f is based on the calculation of the scaling rule, given by Eq. 1:

$$D = -\log N_\varepsilon / \log \varepsilon \quad (1)$$

N_ε being the number of boxes at a certain scale containing part of the image (foreground pixels) and ε the corresponding scale (in pixels).

Lacunarity ($\Lambda\varepsilon$) was calculated as the variation in the number of pixels at each grid placed in the image during a standard box counting, following Eq. 2:

$$\Lambda\varepsilon = \left(\frac{\sigma}{\mu}\right)^2 \quad (2)$$

where $\Lambda\varepsilon$ is the lacunarity for the grid of size ε (in pixels), σ is standard deviation of the pixels count among all boxes of size ε , and μ the average number of pixels for the same grid size. Lacunarity ($\Lambda\varepsilon$) supplements the fractal dimension information by describing the pixels' variation of an image during a standard box count procedure.^{21,22} The higher the lacunarity, the greater is the variation of pixels distribution within an image, indicating higher heterogeneity of the structure. A coefficient of variation (σ/μ) of 0.5 means that the number of pixels per box varies an average of 50% from the mean. A lacunarity greater than 1 means that the standard deviation of the pixels count (σ relative to all positions of boxes in a grid of size ε) exceeds the mean (μ).^{21,22}

Statistical Analysis

Values reported for mechanical properties (stress at rupture, elasticity modulus, and strain at rupture) represent the mean of seven replications obtained for at least two repetitions of each treatment (acidification condition, type, and concentration of polysaccharide), and the error bars represent standard deviation. The SEM images represent the typical structures obtained from at least five replications obtained for a minimum of two repetitions of each treatment. Significant differences ($p < 0.05$) between gels' properties were determined by one-way analysis of variance, and the comparisons between the mean values were evaluated by the Tukey procedure. Statistical analyses were performed using the software STATISTICA 5.5 (Statsoft Inc., Tulsa, USA).

Results

Visual Appearance of the Gels and Mechanical Properties

Lowering the pH of heated whey protein solutions caused the formation of cold-set gels. The gels were studied in pH range between 5.2 and 4.2, corresponding to the isoelectric point of the main whey proteins (5.2 for β -Lg, 4.7 for BSA, and 4.2 for α -La). Preliminary experiments involving measurements of the pH values during acidification time showed that the pH profiles of the mixed protein polysaccharide systems did not exhibit significant differences than those observed for pure protein systems.¹⁰ The gels showed greater variation in pH at the beginning of acidification (first 500 min or 8.3 h), and from this point, the pH values decreased steadily.¹⁰ Such result was attributed to the fact that the acidification conditions implied in slower rate of pH decrease and the gelation kinetics was standardized by modifications in the GDL amount added accordingly to the evaluated system (Table 1). During the first period of acidification, the gel structure development of mixed whey protein polysaccharides systems may be different from those observed for pure whey protein systems, leading to different times of achievement equilibrium of mechanical properties. However, the mixed whey protein polysaccharide systems did not show significant changes ($p < 0.05$) in pH and mechanical properties in periods between 48 and 72 h. Therefore, the equilibrium of mechanical properties of mixed protein-polysaccharide systems were considered at 48 h and the compression experiments were performed at this time.

Pure whey protein gels formed homogeneous and self-supported gels (maintained the form when removed from the plastic tubes) upon acidification and showed a white opaque appearance. Addition of polysaccharides to the WPI solution prior to acidification process led to the formation of gels with different appearance than those observed in pure WPI gels. Mixed WPI-xanthan gels containing 0.1% polysaccharide formed two-phase gels at final pH 5.2. The top phase was turbid, while the bottom phase was white and opaque. The 0.1% xanthan gels at pH 4.2 and 4.7 did not show macroscopic phase separation (completely opaque visual appearance), in the same way of WPI gels with addition of 0.3% or 0.5% of xanthan for all final pH values. The gels composed with guar were homogeneous and opaque with 0.1% and 0.3% polysaccharide concentration for all studied pHs, but in 0.5% of guar, the systems did not form self-supported gels.

The increase in GDL addition in pure WPI gels led to the lower stress at rupture (Figure 1), elasticity modulus (Figure 2) values, and strain at rupture (Figure 3). Such behavior was attributed to a faster and disordered protein aggregation at higher acidification rates, leading to weak structure formation.¹⁰ The formation of disulfide bonds between protein

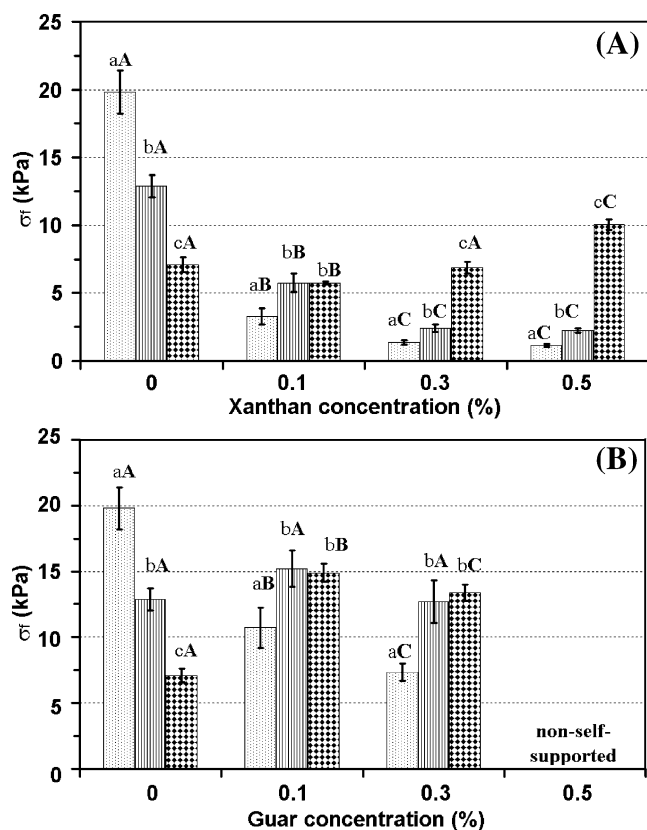


Fig. 1 Stress at rupture (kPa) of 5% WPI cold-set gels with addition of polysaccharides. **a** Xanthan, **b** guar. Gels pH: □ pH 5.2, ▨ pH 4.7 and ▩ pH 4.2. Bars represent standard deviation among replications. Different letters mean significant differences ($p < 0.05$). Small letters, differences amongst the pH gels in each formulation. Capital letters, differences amongst formulations in each pH

aggregates even at the gel state can also be correlated to the stronger and deformable gels obtained at lower acidification rates.^{4,5,11,12} At lower acidification conditions, the protein aggregates had enough time to interact with each other, permitting the cross-link amongst free thiol groups at the surface of the soluble protein aggregates formed during the heat step, but at higher acidification conditions, such aggregates were not formed due to the increase of electrostatic repulsion at lower pH values, which could be related to the weaker gels at pH 4.2.

Although two-layer gel was formed, the 0.1% xanthan gel at pH 5.2 was subjected to compression experiments because they were self-supported. Comparing the values of mixed xanthan gels with the pure whey protein gels, it was observed that xanthan addition caused a decrease in stress at rupture at pH 5.2 and 4.7 (more pronounced decrease at pH 5.2), but in contrast, at pH 4.2, an increase in xanthan concentration caused a slight increase in stress at rupture values (Figure 1a). Such behavior at pH 4.2 was pronounced in elasticity modulus values that showed a sharper increase than for other final pH gels (Figure 2a). The sharper increase of elasticity modulus at pH 4.2 as the

xanthan concentration was increased could be attributed to an increased susceptibility of this parameter to the greater electrostatic interactions among protein and xanthan at final pH 4.2, since elasticity modulus is a parameter determined at lower deformation.

In general, guar addition led to stronger WPI gels than xanthan, and it was observed that at pH 5.2 and 4.2, guar gels showed a decrease in stress at rupture (Figure 1b) in relation to pure whey protein gels. However, at pH 4.7, similar values were obtained at 0.1% and 0.3% guar content. The elasticity modulus of pure whey protein gels has not changed with guar addition at pH 5.2, but an increase in those values for guar gels at pH 4.7 and 4.2 (Figure 2b) was observed. At lower pH, the protein–protein interactions are favored, but at higher concentration of guar (0.5%), a phase separation seems to occur due to an increase in polysaccharide content, which obstructs the protein network formation. This phase separation caused a continuous phase inversion, which means that the system changed from a protein continuous phase to a polysaccharide continuous phase with proteins dispersed along the system as previously observed elsewhere by confocal laser scanning microscopy.⁹

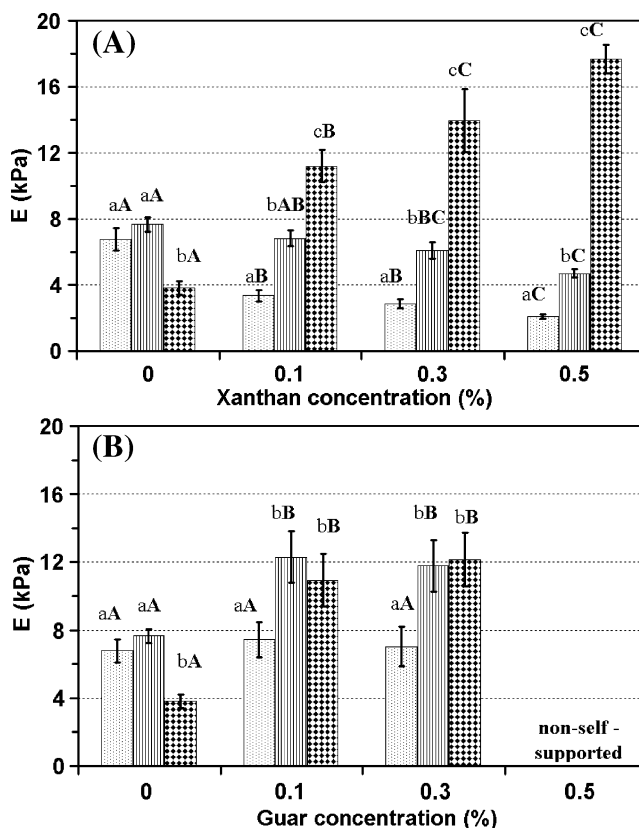


Fig. 2 Elasticity modulus of 5% WPI cold set gels with addition of polysaccharides. **a** Xanthan, **b** guar. Gels pH: □ pH 5.2, ▨ pH 4.7, and ▩ pH 4.2. Bars represent standard deviation among replications. Different letters mean significant differences ($p < 0.05$). Small letters, differences amongst the pH gels in each formulation. Capital letters, differences amongst formulations in each pH

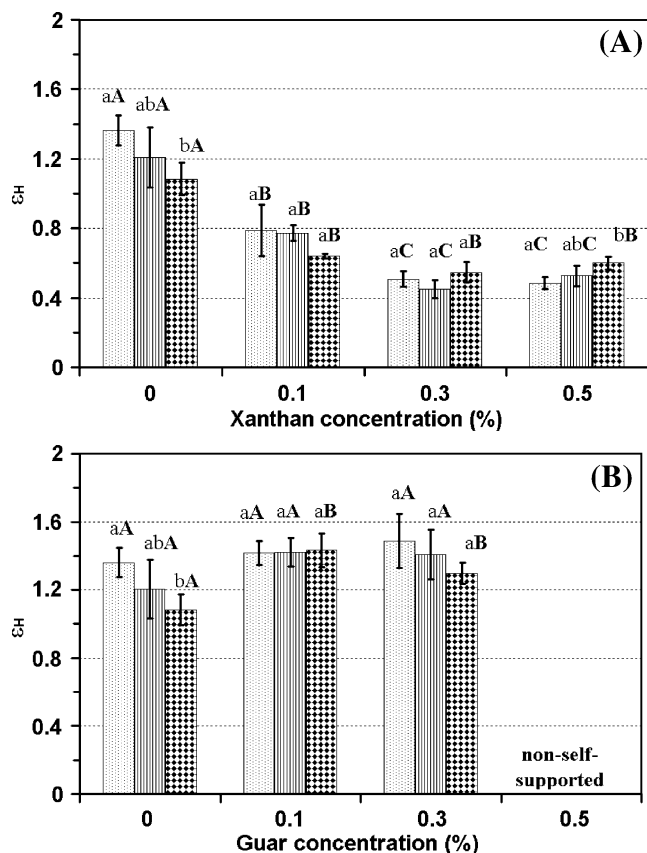


Fig. 3 Strain at rupture of 5% WPI cold-set gels with addition of polysaccharides. **a** Xanthan, **b** guar. Gels pH: □ pH 5.2, ▨ pH 4.7, and ▩ pH 4.2. Bars represent standard deviation among replications. Different letters mean significant differences ($p < 0.05$). Small letters, differences amongst the pH gels in each formulation. Capital letters, differences amongst formulations in each pH

In a general way, the strain at rupture (Figure 3) was not affected by system pH in each polysaccharide concentration, but the addition of xanthan caused a pronounced decrease in the strain values in relation to the pure whey protein gels (Figure 3a). The strain at rupture values of 0.3% and 0.5% xanthan–WPI gels were very similar, showing that the deformability of these gels was almost independent of final pH and xanthan concentration. In contrast, guar self-supported gels were always more deformable than xanthan (Figure 8b) but very similar to pure whey protein gels.

Morphology of the SEM Images Evaluated by Fractal Dimension and Lacunarity

Figure 4 shows the SEM micrographs of pure 5% WPI gels. It is possible to see that a porous and homogeneous structure constituted the pure whey protein gels. This structure was more homogenous with smaller pores at pH 5.2 (Figure 4a) and 4.7 (Figure 4b), while at pH 4.2 (Figure 4c), bigger pores were randomly distributed along the gel network.

Figure 5 shows the obtained microstructure of each macroscopic phase separated of 0.1% xanthan gels at pH 5.2. In Figure 5, it is also possible to observe an example of the 8-bit (binary image) transformation of SEM picture during image analysis, which was necessary to determine the fractal dimension of gels. The top phase showed large, porous, within a 3D branched structure (Figure 5a). The bottom phase showed swallow spherical pores of several diameters distributed along the structure (Figure 5b). In both cases, the pores were significantly marked in the binary images, allowing to outline each pore (binary image in Figure 5). In all evaluated gels, the pores among clusters were pictured as black regions, permitting to set the structures as foreground (white pixels) and pores as background (black pixels). The binary images of each gel were used for the box count method.

Figure 6 shows the 0.1% xanthan gels at pH 4.2 and 4.7 that did not exhibit macroscopic phase separation. A compact and interconnected network was observed, forming branched structures, but with large pores randomly distributed. At pH 4.2, a second structure network of small interconnected spheres also was observed inside the pores, filling the spaces and forming chains and clusters (Figure 6b). The 0.3% xanthan gels showed coarse structure that showed more open pores at pH 5.2 (Figure 7a) than at 4.7 or 4.2 (Figure 7b, c). The 0.5% xanthan gels were more homogeneous and less particulate than at 0.1% or 0.3% xanthan concentration, showing a structure apparently with more pores at pH 5.2 (Figure 7d) than at pH 4.7 and 4.2 (Figure 7e, f, respectively).

The 0.1% guar gels were very similar at the different pH, with round porous randomly distributed (Figures 8a–c).

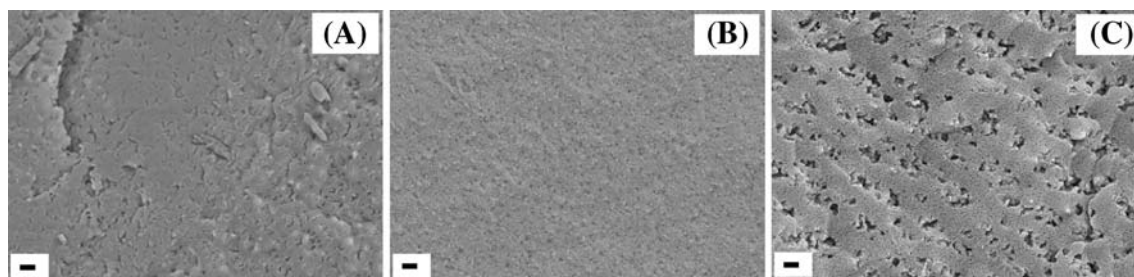
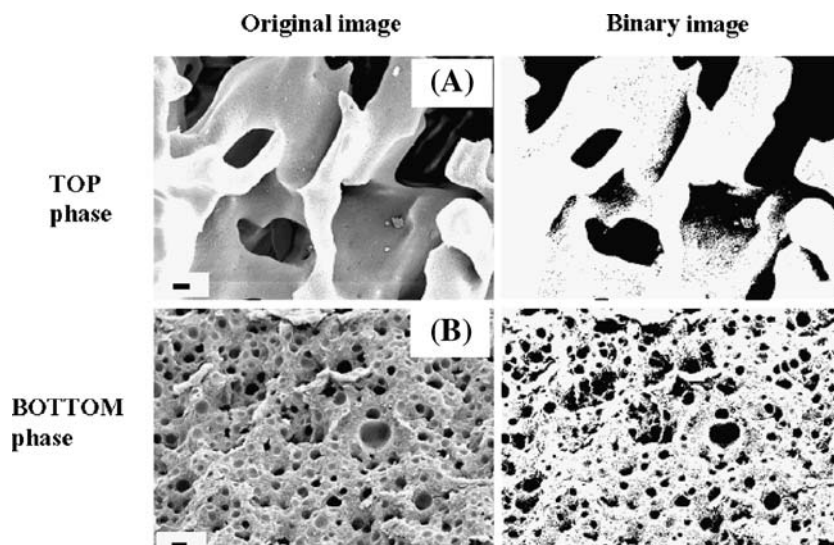


Fig. 4 SEM micrographs of pure 5% WPI acidic cold-set gels. **a** pH 5.2, **b** pH 4.7, and **c** pH 4.2. Scale bar corresponds to 10 μm

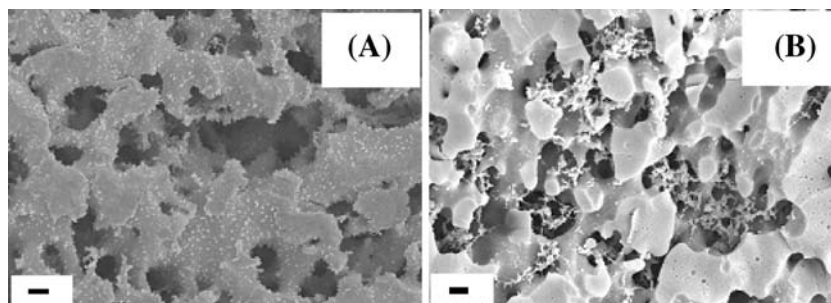
Fig. 5 SEM micrographs (*left*) and corresponding binary images (*right*) of macroscopic phase separated gels of 5% WPI 0.1% xanthan at pH 5.2. Top (a) and bottom (b) phase are outlined. Scale bar corresponds to 10 μm



However, there were more and smaller pores at pH 4.2 (Figure 8c). The addition of larger amounts of guar in the systems caused an increase in the pore size and a clear formation of different structures. At 0.3% guar and pH 5.2 (Figure 8d), a lower amount of pores was visualized, but with larger sizes. A decrease in pore size and its increasing number was observed with a reduction in pH to 4.7 or 4.2. At 0.5% of guar content, the structure was widely open, which could explain the formation of non-self-supported gels (Figure 8g–i).

Average fractal dimensions among 30 image scans (grid positions) for the different systems are shown in Figure 9. Pure whey protein gels were not influenced by system final pH showing similar values ($p < 0.05$) of D_f around 1.8 (at 2D binary images). At pH 5.2 and 0.1% xanthan, the D_f values of top and bottom macroscopic separated phases were quite different from each other. The top phase showed quite smaller D_f than pure whey protein gels at pH 5.2, forming structures with smoother contour lengths. In contrast, the D_f of bottom phase gels were very similar to those for pure whey protein gels at the same pH value (Figure 9a), showing that the latter corresponded to a protein-rich phase. For homogeneous 0.1% xanthan gels, the reduction in pH from 4.7 to 4.2 led to smaller values of D_f , or smoother contour shape of the structure (Figure 9a).

Fig. 6 SEM micrographs of 5% WPI-0.1% xanthan cold-set gels at final pH values. **A** 4.7 and **b** 4.2. Scale bar corresponds to 10 μm



The homogeneous xanthan gels with a concentration 0.1% of polysaccharide showed in general a reduction and an increase in D_f values in relation to pure WPI gels and 0.1% xanthan top phase gel, respectively (Figure 9a), but a further increase in xanthan concentration (0.3% to 0.5%) did not change the D_f values in relation to pure gels. In contrast, the guar addition caused the formation of gel network with smoother surfaces and less rugged than xanthan or pure WPI gels, as observed by the reduction in D_f values. This trend was more pronounced at final pH 5.2, while for pH 4.7 and 4.2, the decrease in D_f values was less sharp (Figure 9b). The greatest reduction in D_f values was observed for 0.3% guar gels for all pH.

Figure 10 shows the lacunarity distribution of pure whey protein gels and mixed WPI–xanthan gels at final pH 5.2 as a function of box size. For the other systems, the lacunarity plot followed a similar trend (data not shown). The lacunarity or heterogeneity of the gels at pH 5.2 increased with the scale until it reaches a box size of approximately 4.5 μm , but 0.1% xanthan top phase gels corresponded to 12 μm (Figure 10). After this maximum point, the heterogeneity reduced until the achievement of steady-state values.

Comparisons among the systems were done by the evaluation of the grid sizes and lacunarity values at the

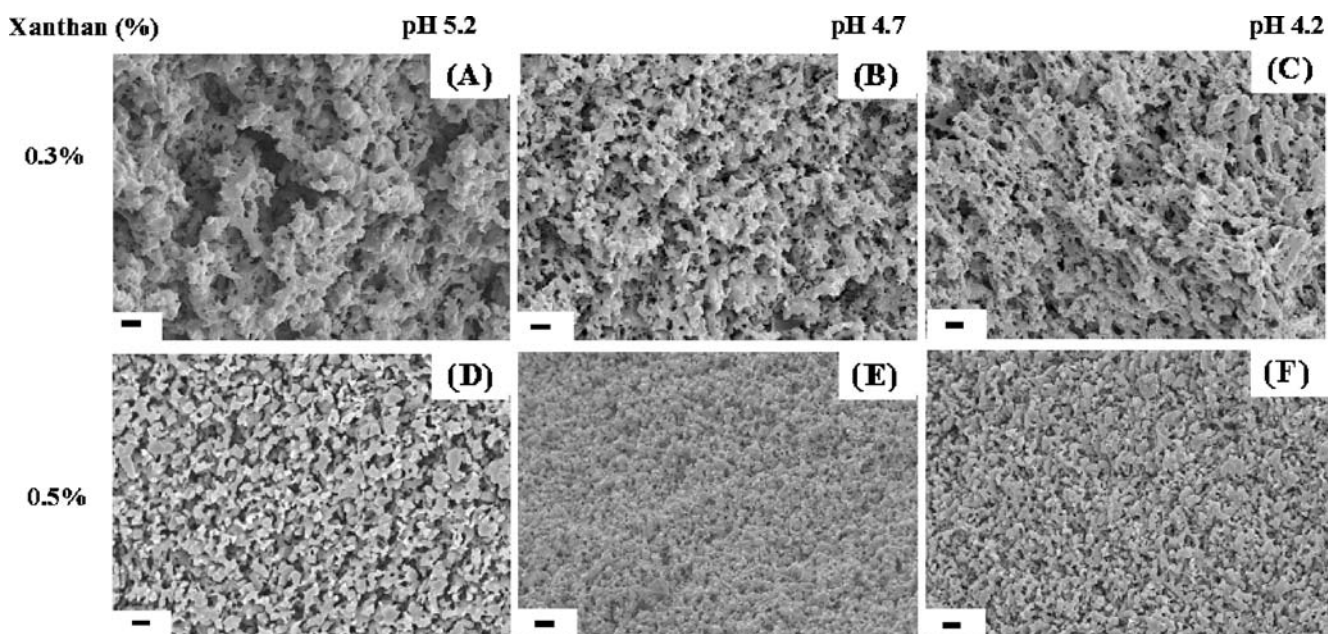


Fig. 7 SEM micrographs of cold-set gels with 5% WPI-xanthan (0.3%, *top row*, and 0.5%, *bottom row*). Final pH values: 5.2 (a, d), 4.7 (b, e), and 4.2 (c, f). *Scale bars* correspond to 10 μm

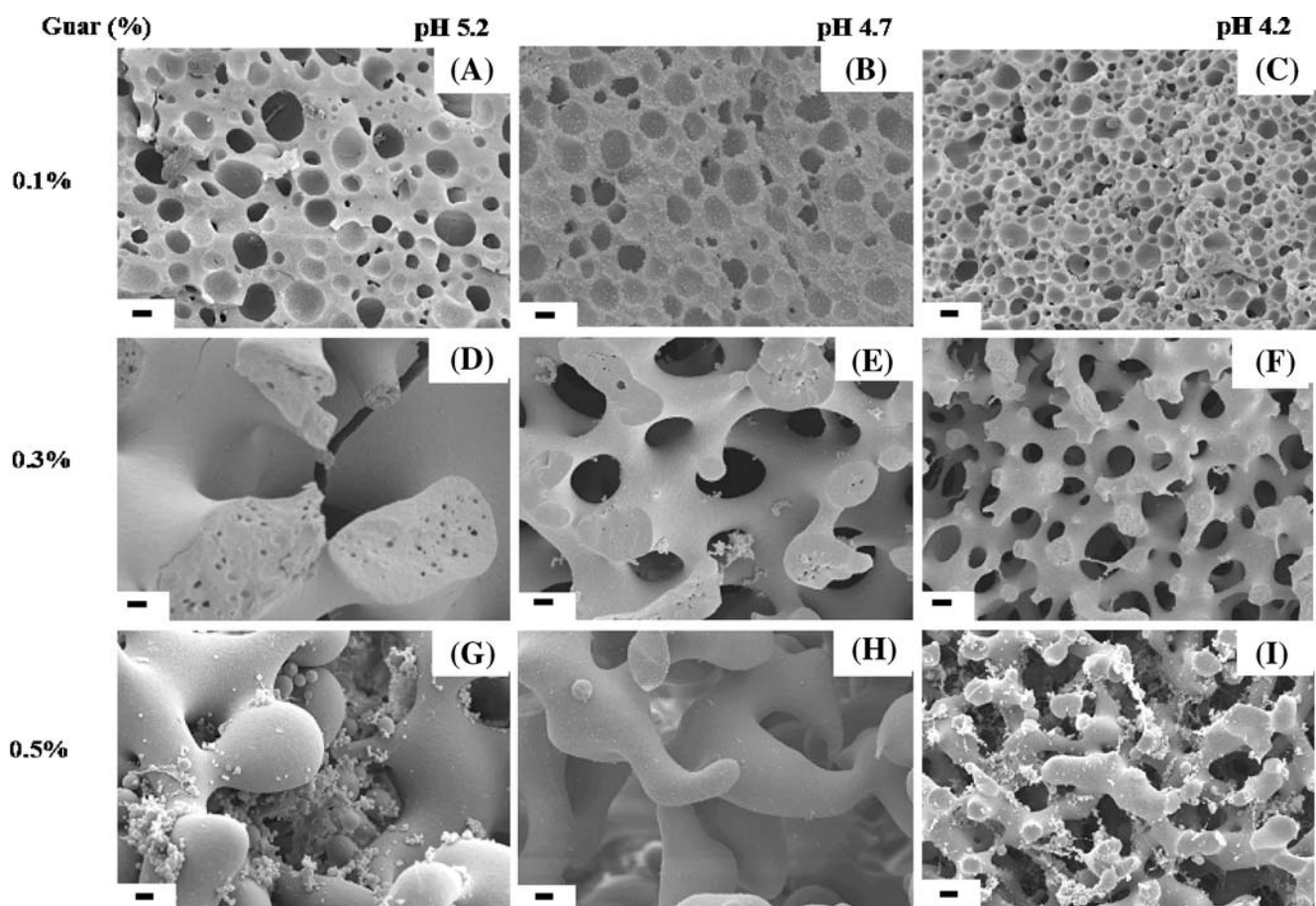


Fig. 8 SEM micrographs of 5% WPI cold-set gels with addition of guar (*top row* are 0.1%, *middle row* are 0.3%, and *bottom row* are 0.5% of guar). Final pH values: 5.2(a, d, g), 4.7 (b, e, h), and 4.2 (c, f, i). *Scale bars* correspond to 10 μm

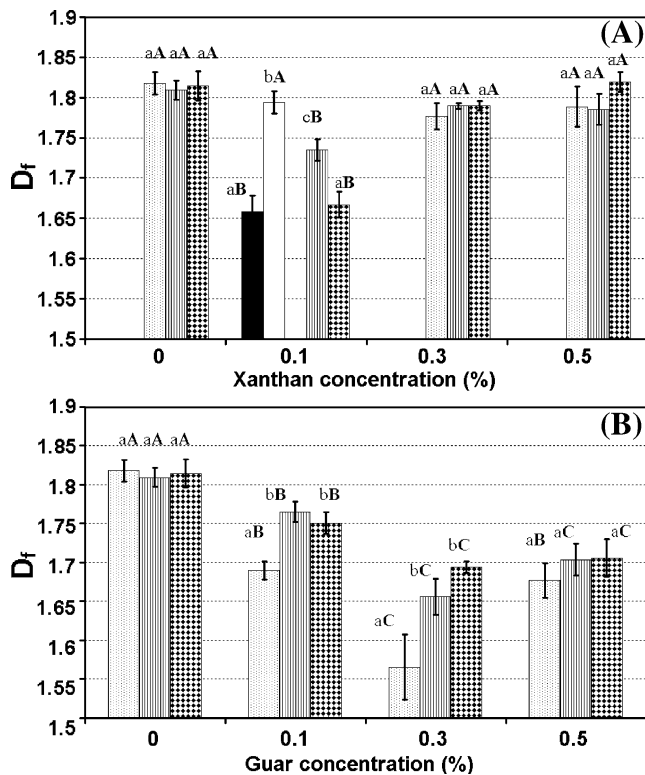


Fig. 9 Fractal dimension of WPI-xanthan (a) and WPI-guar (b) gels. Gels pH: \square 5.2, \blacksquare 4.7 and \boxtimes 4.2. In a, the 0.1% xanthan phase-separated gels at pH 5.2: \blacksquare top phase and \square bottom phase. Bars represent standard deviation from scanning each image in four-grid position. Different letters mean significant differences ($p < 0.05$). Small letters, differences amongst the pH gels in each formulation. Capital letters, differences amongst formulations in each pH

point of maximum heterogeneity of the images. Such a point was selected because it was possible to make a clear distinction among the structures heterogeneity of the different gels, offering a rough idea about the system's porosity. Table 2 shows the values of the grid sizes corresponding to the maximum lacunarity for each gel, and Table 3 shows the lacunarity values at this point.

The maximum lacunarity of pure whey protein gels was described during the box count procedure by boxes of grid sizes around $2.3 \mu\text{m}$, and significant differences among the different final pH gels were not observed. The addition of polysaccharides led to a modification of the heterogeneity distribution of the microstructure in relation to the grid sizes. For xanthan gels, the heterogeneity was greater at final pH 5.2 and 0.1% of polysaccharide addition showing the greater values of grid sizes and lacunarity (Tables 2 and 3, respectively). Such characteristic of heterogeneity was greater for top phase xanthan gels, but the increase of xanthan concentration and the reduction of final pH led to a reduction of the parameters of heterogeneity to values relatively similar to those of pure whey protein gels. The increase in this guar concentration led to an opposite trend as

compared to xanthan gels, which is visualized with grid size values (Table 2). On the other hand, the reduction of final pH for guar gels did not show a clear tendency of heterogeneity parameters. However, it is noteworthy that the increase of polysaccharide concentration led to a decrease of lacunarity (Table 2) or porosity (Figures 7 and 8), but for guar gels, this parameter showed greater values, which can be associated with the higher tendency to phase separation.

Discussion

The obtained results suggest that the increase or decrease in structure discontinuity (porosity) in WP cold-set gels due to polysaccharide addition can be attributed to an obstruction of protein-protein interaction by the polysaccharide. Such a fact is obviously related to the kind of thermodynamic interaction occurring among WP thermal aggregates and each polysaccharide during the process of gel formation, but the different acidification conditions also exerted a clear influence on system microstructure. The latter could be attributed to the competition between the simultaneous process of gelation and biopolymers incompatibility (phase separation) occurring during pH decay, mainly at the initial phase of acidification process. Thus, three factors associated with the gel formation process should be considered: (1) the phase separation that was more relevant close to neutral pH and/or above the WP pI (beginning of the acidification), (2) the rate of pH decrease, and (3) the value of the gel final pH. Thermodynamic incompatibility between the biopolymers prevailed at the beginning of acidification over the protein aggregation. In the case of xanthan, such an incompatibility is in great part related to the similar charge of xanthan and WP thermal aggregates at neutral pH.²³ For the neutral guar gum, the incompatibility is strongly related to the mutual exclusion of accessible volume of mass of biopolymers, which is known as exclusion volume ef-

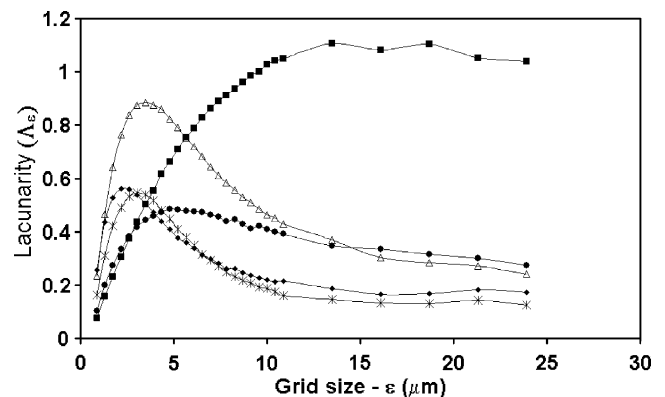


Fig. 10 Typical lacunarity plot from SEM binary images of the cold set gels at pH 5.2. \blacklozenge pure WPI, WPI-xanthan gels: \blacksquare 0.1% top phase, \triangle 0.1% bottom phase, \bullet 0.3%, and \ast 0.5%

Table 2 Grid box size in micrometers at maximum lacunarity values

pH	Whey protein	Xanthan			Guar		
		0.1% (w/w)	0.3% (w/w)	0.5% (w/w)	0.1% (w/w)	0.3% (w/w)	0.5% (w/w)
5.2	2.3±0.2 ^(aA)	Top phase=17.5±2.4 ^(aB) Bottom phase=3.7±0.3 ^(bC)	4.6±0.4 ^(aD)	3.2±0.3 ^(aE)	6.4±0.5 ^(aB)	21.6±0.2 ^(aC)	25.2±0.0 ^(aD)
4.7	2.3±0.5 ^(aA)	10.9±1.8 ^(cB)	3.7±0.2 ^(bC)	2.6±0.0 ^(aD)	5.4±0.9 ^(aB)	19.2±1.1 ^(bC)	56.1±6.1 ^(bD)
4.2	1.7±0.0 ^(aA)	9.6±0.7 ^(cB)	3.1±0.5 ^(bC)	2.4±0.3 ^(aC)	4.9±0.7 ^(aB)	11.1±1.0 ^(cC)	8.5±1.3 ^(cD)

Different letters mean significant differences ($p < 0.05$). Small letters: differences amongst the pH gels in each formulation. Capital letters: differences amongst formulations in each pH

fect.^{24,25} The period in which the systems are kept at pH > pI is longer for systems formed at lower acidification rates.^{10,12} In such a condition (final pH value corresponding to 5.2), the thermodynamic incompatibility was favored among the biopolymers during acidification and also in the final pH, as α -La and BSA (almost 20% of WP in WPI) were still negatively charged, resulting in a more discontinuous structure. This assumption was corroborated by the clear macroscopic phase separation of 0.1% xanthan gels at pH 5.2. In this case, phase separation was favored due to the low initial viscosity of such systems (lower biopolymer concentration), allowing a higher biopolymer mobility.²³ This latter hypothesis is confirmed by the fact that no macroscopic phase separation was observed in gels with pH 5.2 and higher xanthan content, which have higher viscosity before acidification. At the highest GDL ratio, the gelation rate was faster than the phase separation due to the intensified rate of pH decrease, but in such condition, there was not enough time for protein aggregation and rearrangements close to the β -Lg and BSA pI s. Moreover, by adding xanthan, the protein–protein interactions were probably even more obstructed due to a decrease in system mobility. On the other hand, at pH 4.2 some WP (β -Lg and BSA) had predominantly positive charge, favoring electrostatic protein–polysaccharide interactions, which was associated with the more continuous network at this final pH.

The excluded volume effects in WPI–guar mixed gels were more intense at higher polysaccharide contents, which resulted in gel microstructure discontinuity and non-

self-supported gel formation. Probably, at lower polysaccharide concentrations, WP thermal aggregates and guar exhibited microscopic phase separation,⁹ but the high viscosity of the system at the beginning of the acidification process probably obstructed the macroscopic phase separation, leading to the formation of visually homogeneous gels.

In both cases (WPI–xanthan or WPI–guar), the result was the formation of rich protein and depleted protein zones in the microstructure or rich polysaccharide zones. These effects were visualized by Sanchez et al.²⁶ in skim milk acidified gels with addition of locust bean gum and/or xanthan. These authors related the formation of discontinuous microstructure due to depletion enrichment of protein and polysaccharide zones on gel microstructure. As a consequence, the gel porosity was increased in the presence of polysaccharides. The increase in system porosity was related to a condensation and localized increase in casein network density in regions of the gels' microstructure. de Jong and van de Velde⁹ studied the microstructure of WPI cold-set gels with addition of galactomannans or xanthan at a fixed acidification rate. They used confocal laser microscopy to demonstrate that the polysaccharides (specially the galactomannan) led to a condensation of the protein network and increase in system porosity.

Besides the narrow range of D_f variation, the values obtained allowed describing the structural differences among the studied gels, especially concerning the effects of polysaccharide addition to the microstructure. Previous works have evaluated fractal dimension of pure protein gels

Table 3 Maximum values of lacunarity of the WPI cold-set gels with addition of polysaccharides

pH	Whey protein	Xanthan			Guar		
		0.1% (w/w)	0.3% (w/w)	0.5% (w/w)	0.1% (w/w)	0.3% (w/w)	0.5% (w/w)
5.2	0.56±0.01 ^(aA)	Top phase=1.23±0.07 ^(aB) Bottom phase=0.86±0.03 ^(bC)	0.59±0.08 ^(aA)	0.57±0.03 ^(aA)	1.02±0.19 ^(aAB)	1.26±0.30 ^(aB)	0.75±0.01 ^(aAB)
4.7	0.62±0.07 ^(aA)	0.87±0.02 ^(bB)	0.52±0.03 ^(aA)	0.64±0.03 ^(aA)	1.15±0.27 ^(aB)	0.87±0.11 ^(bAB)	0.66±0.03 ^(aA)
4.2	0.64±0.16 ^(aA)	0.88±0.12 ^(bB)	0.52±0.02 ^(aA)	0.48±0.03 ^(bA)	0.93±0.17 ^(aA)	0.72±0.03 ^(bA)	0.59±0.14 ^(aA)

Different letters mean significant differences ($p < 0.05$). Small letters: differences amongst the pH gels in each formulation. Capital letters: differences amongst formulations in each pH

in several ways, including rheology, permeability measurements, light scattering, and microscopy.^{27–29} However, the measurements of D_f using the image analysis were very important since rheological models fail to correlate the particle concentration with the elastic constants of phase-separated protein–polysaccharide systems.

The use of the scaling models to determine the fractal dimensions in terms of the relation between gel elasticity and biopolymer concentration have some limitations in describing the aggregation of mixed protein and polysaccharide acidified systems. These limitations arise considering that mixed protein and non-gelling polysaccharides (xanthan or guar) lead to an irregular aggregation behavior that is independent of the increase in biopolymer concentration differently of pure protein systems formed upon heating^{21,22,28,29}, salt addition,³⁰ acidification,³¹ or enzyme addition.^{32–34} The obtained phase-separated gels did not exhibit an increased behavior in log–log plot of elasticity to particle concentration due to the predominance of phase separation over the gelation or protein aggregation. However, the models could in part work at conditions where the aggregation was favored.

The patterns of D_f values for guar gels (Figure 9b) and stress at rupture or elasticity modulus (Figures 1 and 2b, respectively) showed a similar trend in relation to guar concentration or final pH of gel. This could show a correlation between the mechanical properties and D_f as a microstructure quantification parameter. However, these correlations were difficult to observe for xanthan gels, since the variability in microstructure patterns was very intense, especially at lower polysaccharide concentration where macroscopic phase separation was evident. In addition, higher xanthan concentration entailed an increase of D_f values similar to pure whey protein gels, but an increase in mechanical property attributes in a similar way was not observed. Thus, the 2D fractal dimension values could be used as indicative of the contour length complexity of the gel network in binary images, as higher D_f values indicated high degree of ruggedness and very tortuous structure silhouette.³⁵

Since fractal dimension was not enough to provide a complete distinction among the different structures obtained as a function of the prevailing gelation or phase separation mechanism, an additional parameter was necessary to describe the changes in the microstructure. Lacunarity parameters complemented the fractal dimension information and were used to report variations in the image associated with the structure heterogeneity. The results showed that the grid sizes that described the maximum values of lacunarity (Table 2) showed the differences among the microstructures, while the lacunarity values (Table 3) offered an idea of the degree of microstructure variability. It is like saying that if the maximum of lacunarity values was reached at small scales,

the largest variability is related to small cavities. In contrast, maximum of lacunarity values at bigger grid sizes are related to greater cavities. For systems where phase separation was the prevailing mechanism, greater grid sizes to describe the heterogeneity during the box count procedure were necessary. In this way, greater grid sizes were necessary to describe the maximum heterogeneity of low concentration xanthan gels at final pH 5.2 or higher concentration guar gels.

Conclusion

The results obtained in this study showed that addition of xanthan or guar to whey protein solutions before the system acidification led to a great modification of properties of whey protein isolate cold-set gels. Such modifications depended strongly on polysaccharide type and concentration, acidification condition, and final pH of the gel. Despite the specific differences of biopolymer interactions of each polysaccharide used, the results suggest that in both types of mixed gels, the final properties were a result of a competition among two or three phenomena that occurred simultaneously during the acidification process: (1) segregative phase separation at initial step of acidification, (2) gelation resultant from the reduction of pH towards the pI of the main WP, and (3) aggregative interactions between the positively charged proteins ($pH < pI$) and negatively charged polysaccharide at final pH. In the case of WPI–xanthan gels, gelation occurred simultaneously to the biopolymers' incompatibility due to the similar charge of xanthan and WP thermal aggregates at neutral pH, while for WPI–guar gels, the incompatibility was probably related to exclusion volume effects. At lower acidification rates and higher final pH, phase separation phenomenon was favored due to an increased time of system permanence at pH values higher than the BSA and α -La pI , (prevailing the negatively charge of the main WP), resulting in an increase of microstructure porosity and weaker gels. In contrast, at higher acidification conditions and lower final pH, gelation phenomena was predominant, favoring the structure formation with lower porosity. As a result, mixed gels with stronger structure were produced. The image analyses were important to quantitatively describe the great variety of microstructure attributes in terms of the fractal dimension and lacunarity. Fractal dimension values ranged between 1.55 and 1.85 and were dependent on pH and xanthan concentration, while for WPI–guar gels, they were only influenced by the polysaccharide concentration. The correlation among fractal dimension and the system's mechanical properties was not clear, which was in part related to the narrow range of scale variation; however, fractal analysis was relevant to measure the degree of complexity in the 2D binary images. Lacunarity analysis complemented structure evaluation and was performed to

study the distribution of heterogeneity of the gels, mainly attributed to pores within the gels' microstructure.

Acknowledgments This research was supported by FAPESP (04/08517-8) and CNPq (301869/2006-5 and 140506/2003-9).

References

1. A.H. Clark, G.M. Kavanagh, S.B. Ross-Murphy, *Food Hydrocoll.* **15**, 383–400 (2001). doi:10.1016/S0268-005X(01)00042-X
2. C.M. Bryant, D.J. McClements, *Trends Food Sci. Technol.* **9**, 143–151 (1998). doi:10.1016/S0924-2244(98)00031-4
3. Z.Y. Ju, A. Kilara, *J. Agric. Food Chem.* **46**, 1830–1835 (1998). doi:10.1021/jf9710185
4. A.C. Alting, H.H.J. de Jongh, R.W. Visschers, J. Simons, *J. Agric. Food Chem.* **50**, 4682–4689 (2002). doi:10.1021/jf011657m
5. A.C. Alting, R.J. Hamer, C.G. De Kruif, M. Paques, R.W. Visschers, *Food Hydrocoll.* **17**, 469–479 (2003). doi:10.1016/S0268-005X(03)00023-7
6. A.C. Alting, R.J. Hamer, C.G. De Kruif, R.W. Visschers, *J. Agric. Food Chem.* **51**, 3150–3156 (2003). doi:10.1021/jf0209342
7. A. Syrbe, W.J. Bauer, N. Klostermeyer, *Int. Dairy J.* **8**, 179–193 (1998). doi:10.1016/S0958-6946(98)00041-7
8. S. de Jong, H. Jan Klok, F. van de Velde, *Food Hydrocoll.* **23**, 755–764 (2009). doi:10.1016/j.foodhyd.2008.03.017
9. S. de Jong, F. van de Velde, *Food Hydrocoll.* **21**, 1172–1187 (2007). doi:10.1016/j.foodhyd.2006.09.004
10. A.L.F. Cavallieri, R.L. Da Cunha, *Food Hydrocoll.* **22**, 439–448 (2008). doi:10.1016/j.foodhyd.2007.01.001
11. A.C. Alting, R.J. Hamer, G.G. de Kruif, R.W. Visschers, *J. Agric. Food Chem.* **48**, 5001–5007 (2000). doi:10.1021/jf000474h
12. A.L.F. Cavallieri, A.P. Costa-Netto, M. Menossi, R.L. Da Cunha, *Lait* **87**, 535–554 (2007). doi:10.1051/lait:2007032
13. W.C. Wielinga, in *Galactomannans*, ed. by G.O. Phillips, P.A. Williams. *Handbook of Hydrocolloids* (CRC, Boca Raton, 2000), pp. 153–171
14. G. Swom, in *Xanthan gum*, ed. by G.O. Phillips, P.A. Williams. *Handbook of Hydrocolloids* (CRC, Boca Raton, 2000), pp. 179–193
15. U.K. Laemmli, *Nature* **227**, 680–685 (1970). doi:10.1038/227680a0
16. J.R. Hodge, B.T. Hofreiter, in *Determination of reducing sugars and carbohydrates: Phenol Sulfuric test*, ed. by R.L. Wistler, M.L. Wolfman. *Methods in Carbohydrate Chemistry* (Academic, New York, 1962), pp. 380–394
17. AOAC., *Official Methods of Analysis of AOAC international. Association of Official Analytical Chemists* (Patricia Cunniff, Gaithersburg, USA, 1997)
18. J.F. Steffe, *Rheological Methods in Food Process Engineering* (Freeman, East Lansing, USA, 1996)
19. L.A. Pagnaloni, L. Matia-Merino, E. Dickinson, *Colloid. Surf. B.* **42**, 211–217 (2005). doi:10.1016/j.colsurfb.2005.03.002
20. B.H. Kaye, *A Random Walk Through Fractal Dimensions* (VHC Verlagsgesellschaft, Weinheim, Germany, 1989)
21. E. Davila, M. Toldra, E. Saguero, C. Carretero, D. Pares, *LWT-Food Sci. Technol.* **40**, 1321–1329 (2007)
22. E. Dávila, D. Perés, *Food Hydrocoll.* **21**, 147–153 (2007). doi:10.1016/j.foodhyd.2006.02.004
23. C.M. Bryant, D.J. McClements, *Food Hydrocoll.* **14**, 383–390 (2000). doi:10.1016/S0268-005X(00)00018-7
24. D.V. Zasytkin, E.E. Braudo, V.B. Tolstoguzov, *Food Hydrocoll.* **11**, 159–170 (1997)
25. V. Tolstoguzov, *Food Hydrocoll.* **17**, 1–23 (2003). doi:10.1016/S0268-005X(01)00111-4
26. C. Sanchez, R. Zuniga-Lopez, C. Schmitt, S. Despond, J. Hardy, *Int. Dairy J.* **10**, 199–212 (2000). doi:10.1016/S0958-6946(00)00030-3
27. M. Langton, A.M. Hermansson, *Food Hydrocoll.* **10**, 179–191 (1996)
28. T. Hagiwara, H. Kumagai, K. Nakamura, *Food Hydrocoll.* **12**, 29–36 (1998). doi:10.1016/S0268-005X(98)00043-5
29. T. Hagiwara, H. Kumagai, T. Matsunaga, *J. Agric. Food Chem.* **45**, 3807–3812 (1997). doi:10.1021/jf970348m
30. A.G. Marangoni, S. Barbut, S.E. McGauley, M. Marcone, S.S. Narine, *Food Hydrocoll.* **14**, 61–74 (2000). doi:10.1016/S0268-005X(99)00046-6
31. M. Mellema, J.H.J. van Opheusden, T. van Vliet, *J. Rheol. (NYNY)* **46**, 11–29 (2002). doi:10.1122/1.1423311
32. M. Mellema, P. Walstra, J.H.J. van Opheusden, T. van Vliet, *Adv. Colloid. Interface Sci.* **98**, 25–50 (2002). doi:10.1016/S0001-8686(01)00089-6
33. Q.X. Zhong, C.R. Daubert, O.D. Velev, *Langmuir* **20**, 7399–7405 (2004). doi:10.1021/la036147w
34. Q.X. Zhong, C.R. Daubert, O.D. Velev, *J. Agric. Food Chem.* **55**, 2688–2697 (2007). doi:10.1021/jf0625914
35. A. Barret, M. Peleg, *Food Sci. Technol.-Lebensm.-Wiss. Technol.* **28**, 553–563 (1995). doi:10.1016/0023-6438(95)90001-2